Applied Clay Science 134 (2016) 210–220

Contents lists available at ScienceDirect

Applied Clay Science

journal homepage: www.elsevier.com/locate/clay

Research paper

Chlorite geothermometry applied to massive and oscillatory-zoned radiated Mn-rich chlorites in the Patricia Zn-Pb-Ag epithermal deposit (NE, Chile)

Darío Chinchilla [a,b,*], Xabier Arroyo [c], Raúl Merinero [a], Rubén Piña [a], Fernando Nieto [d], Lorena Ortega [a], Rosario Lunar [a,b]

[a] Departamento de Cristalografía y Mineralogía, Facultad de Ciencias Geológicas, Universidad Complutense de Madrid, C/ José Antonio Nováis, 12, 28040 Madrid, Spain
[b] Instituto de Geociencias (CSIC, UCM), Facultad de Ciencias Geológicas, Universidad Complutense de Madrid, Spain
[c] CAI de Técnicas Geológicas, Facultad de Ciencias Geológicas, Universidad Complutense de Madrid, C/ José Antonio Nováis, 12, 28040 Madrid, Spain
[d] Departamento de Mineralogía y Petrología, Instituto Andaluz de Ciencias de la Tierra, Universidad de Granada-CSIC, Avenida Fuentenueva, 18002 Granada, Spain

ARTICLE INFO

Article history:
Received 16 March 2016
Received in revised form 30 September 2016
Accepted 6 October 2016
Available online 13 October 2016

Keywords:
Oscillatory-zoned chlorite
Radiated chlorite
Epithermal deposit
Mn-rich chlorite
Geothermometer

ABSTRACT

Two textural types of chlorite are identified in the mineralised veins at the Patricia Zn-Pb-Ag epithermal ore deposit (NE, Chile): massive and oscillatory-zoned radiated chlorites. Three main stages of mineralisation have been defined in the Patricia deposit: (1) pre-ore stage, (2) base-metal stage which is divided into two substages: substage 2a and substage 2b and (3) post-ore stage. Both types of chlorite are classified as chamosite and occur coeval to the sphalerite precipitation during the substage 2a. Massive chlorite shows an average content of 33 wt.% FeO, 4.9 wt.% MnO, and 4 wt.% MgO. Oscillatory zoning in radiated chlorites consists of concentric bands with different contents on FeO (from 26.45 to 41.41 wt.%), MgO (from 1.7 to 5.44 wt.%) and MnO (from 1.7 to 9.32 wt.%). Four different chlorite geothermometers based on the system SiO_2-Al_2O_3-FeO-MgO-H_2O were applied to both types of chlorites. The temperature estimations are in agreement with temperatures data of fluid inclusions previously measured in sphalerite of the sub-stage 2a. Despite the high content in Mn of chlorites, the study confirms the applicability of the chlorite geothermometers without the knowledge of the Fe^{3+}/Fe ratio in low-pressure paragenesis and its usefulness as an important tool for characterising the thermal conditions in epithermal ore deposits.

1. Introduction

Temperature and pressure of mineralising fluids are essential parameters to characterise ore forming processes in hydrothermal systems. Changes in chemical and/or physical conditions during the sequence of mineralisation are reflected in banded veins and comb, crustiform and colloform textures as well as compositionally zoned minerals. Several methods are commonly used to trace thermal variations within hydrothermal systems, including fluid inclusions studies, stable isotopes and mineral geothermometry. However, careful paragenetic determinations on the mineralogical assemblage are essential for obtaining meaningful results from the geothermometric methods.

Chlorite mineral group is a typical phyllosilicate in most diagenetic, metamorphic and altered rocks. It can crystallise at different temperature conditions (Hayes, 1970; De Caritat et al., 1993; Walker, 1993) ranging from 40 °C in diagenetic sandstones (Hillier and Velde, 1991) to 600 °C in high-grade metapelites (Vidal et al., 2001). The chemical composition of chlorite is sensitive to pressure (P) and temperature (T) of formation. Therefore, several methods have been elaborated to estimate these P-T conditions (Cathelineau, 1988; Hillier and Velde, 1991; Walshe, 1986; Vidal et al., 2001, 2005, 2006; Parra et al., 2005; Inoue et al., 2009, 2010). Recently, Bourdelle et al. (2013) and Lanari et al. (2014) have published three new geothermometers based on thermodynamic criteria. Using these methods, chlorite has been effectively used as geothermometer in different geological contexts (e.g. Kranidiotis and MacLean, 1987; De Caritat et al., 1993; Vidal et al., 2006; Dora and Randive, 2015; Bourdelle and Cathelineau, 2015; Trincal et al., 2015) including also geothermal systems (Cathelineau and Nieva, 1985; Inoue et al., 2010; Rae et al., 2011; Vazquez et al., 2014).

The first geothermometers (e.g. Cathelineau and Nieva, 1985; Cathelineau, 1988) were based on empiric estimations, comparing the chemical composition found in a particular case with the temperature known for such cases by independent criteria. Such approaches were highly criticised due to the high influence of interstratifications and

* Corresponding author at: Departamento de Cristalografía y Mineralogía, Facultad de Ciencias Geológicas, Universidad Complutense de Madrid, C/ José Antonio Nováis, 12, 28040 Madrid, Spain.
E-mail address: dchinchilla@geo.ucm.es (D. Chinchilla).

http://dx.doi.org/10.1016/j.clay.2016.10.013
0169-1317/

intergrowths on the apparent determined composition (Essene and Peacor, 1995) and the significant dependence on the chemical composition of the system in which the chlorite had formed (Xie et al., 1997; López-Munguira et al., 2002; De Caritat et al., 1993). The conclusion was that such geothermometric approaches could be valid only for a given geological context (Vidal et al., 2016). More recently, geothermometry based on fully thermodynamic approaches was developed (e.g. Vidal et al., 2005, 2006; Inoue et al., 2009, 2010), integrating and refining the validity and limitations of the previous geothermometric experience. The principal problem of application of these methods was the need of the knowledge of the Fe^{2+}/Fe^{3+} ratio in chlorite. The new geothermometers developed by Bourdelle et al. (2013) and Lanari et al. (2014) and its graphical application by Bourdelle and Cathelineau (2015) obey this problem by the combination of the thermodynamic calculation with a semiempirical approach based in a big database of compositions of chlorites. In practice, the two methods use an average Fe^{2+}/Fe^{3+} ratio implicit in the compositional database and consequently accept an inherent level of error (around 50 °C) linked to the lack of the Fe^{2+}/Fe^{3+} ratio data for each particular case. One limiting problem of the geothermometers used until now is that they have been developed only for chlorites in the system SiO_2-Al_2O_3-FeO-MgO-H_2O, with no consideration of other minor components as e.g. Mn, Ni, and Zn, which, in some particular mineral deposits may become significant components of chlorite.

In this contribution we present a detailed study of the texture, mineralogy and geochemistry of Mn-rich chlorites which has been directly formed from the mineralising fluids in the Patricia Zn-Pb-Ag epithermal ore deposit, the only example known to date of this type of mineralisation within the late Eocene-Oligocene metallogenic belt in northeastern Chile (Chinchilla et al., 2016). The objective of this study is to check the use of chlorite as geothermometer in this mineralisation, applying the methods of Vidal et al. (2005, 2006), Inoue et al. (2009, 2010), Bourdelle et al. (2013) and Lanari et al. (2014) and contrasting the results with fluid inclusions data (Chinchilla et al., 2016). This approach allows the more suitable chlorite geothermometric methods to be discussed for the Patricia deposit and,

Fig. 1. Location of the Patricia Zn-Pb-Ag epithermal deposit and other Cenozoic deposits and prospects within major metallogenic belts of northern Chile and southern Peru (modified from Camus and Dilles, 2001).

therefore, to evaluate the possibility of extending the use of chlorite as geothermometer in the research of epithermal ore deposits.

2. Regional geology and mineralogical background of the Patricia epithermal ore deposit

At a regional scale, the formation of the Patricia ore deposit is associated to an orogenic belt (Andean Cordillera) in a convergent margin due to the subduction of successive oceanic plates (i.e. Farallon plate until ca. 23 Ma, Nazca plate since then; Silver et al., 1998; Lonsdale, 2005) beneath the continental margin of the South American Plate. During the subduction process, there are periods dominated by enhanced arc/back-arc development during which plutons and ore deposits were emplaced under an extensional regime (Martinod et al., 2010). The Patricia ore deposit is located in the Central Andes where several long and linear, orogen-parallel metallogenic belts have been defined, each one developed during distinct metallogenic epochs from Cretaceous to Early Oligocene times (Camus and Dilles, 2001). These metallogenic belts contains the largest concentration of Cu resources in the world, mostly in the form of world-class porphyry copper deposits such as Chuquicamata, El Teniente, La Escondida and El Salvador (Behn et al., 2001; Sillitoe and Perelló, 2005; Maksaev et al., 2007) (Fig. 1).

The Patricia ore deposit is a Zn-Pb-Ag mineralisation associated to Andean volcanism consistent with an intermediate sulfidation epithermal deposit (Chinchilla et al., 2016) and representing the only example known to date of this type of mineralisation within the late Eocene-Oligocene metallogenic belt in northeastern Chile (Fig. 1). The ore body is hosted by volcano-sedimentary units (tuffaceous and andesitic breccias) and consists of a set of subvertical E-W vein systems internally comprising stockworks with veinlets from 1 to 10 cm wide, striking NW-SE, E-W and NE-SW, and mostly showing steep inclinations. Veinlets present typical open-space filling textures, including both symmetric and asymmetric banding and comb structures. Evidence of episodic mineral precipitation, with changes in the physicochemical conditions of mineralisation, is recorded both at the veinlet scale by layers with different paragenesis and at the mineralogical scale by the development of banding or zoning textures as those exhibited by quartz, pyrite, arsenopyrite, sphalerite and chlorite (Chinchilla et al., 2013, 2015). Furthermore, the dynamic features of the tectonic environment are indicated by the episodic opening of earlier veinlets and the development of new ones, each recording different parts of the whole paragenetic sequence (Chinchilla et al., 2016).

Three main stages of mineralisation have been defined (Chinchilla et al., 2016): (1) Pre-ore stage characterised by early quartz, pyrite and arsenopyrite; (2) base-metal and silver stage, divided into two substages: 2a characterised by sphalerite and minor amounts of chalcopyrite and pyrrhotite; and 2b characterised by abundant brecciation and the formation of sphalerite and galena, and minor chalcopyrite, pyrrhotite and Ag-bearing minerals; and (3) post-ore stage characterised by late quartz, kutnohorite and minor sulfides (arsenopyrite, sphalerite, pyrite, galena, Ag-bearing minerals and Pb-sulfosalts). Temperatures estimated from fluid inclusions for these three stages ranged from 210 to 250 °C in the pre-ore stage; from 150 to 250 °C in the base metal and silver stage; and from 175 to 215 °C for the post-ore stage (Chinchilla et al., 2015).

3. Sample selection, preparation and methods

In order to carry out a detailed study of textures, microstructures, mineralogy and geochemical variability of chlorite, 22 representative vein samples containing abundant chlorite from 12 drill cores were selected. A semi-quantitative determination of the mineralogy of these 22 vein samples was performed by X-ray diffraction (XRD) using a Bruker D8 Advance diffractometer equipped with a Sol-X detector at the Research Support Centre of Geological Techniques of the Complutense University of Madrid. The bulk mineralogy was determined in randomly oriented powders, and the mineralogy of clay minerals in oriented aggregates mounts prepared with the <2 μm fraction. The <2 μm fraction was extracted from an aqueous suspension according to Stoke's law (Moore and Reynolds, 1989). These oriented aggregates mounts were

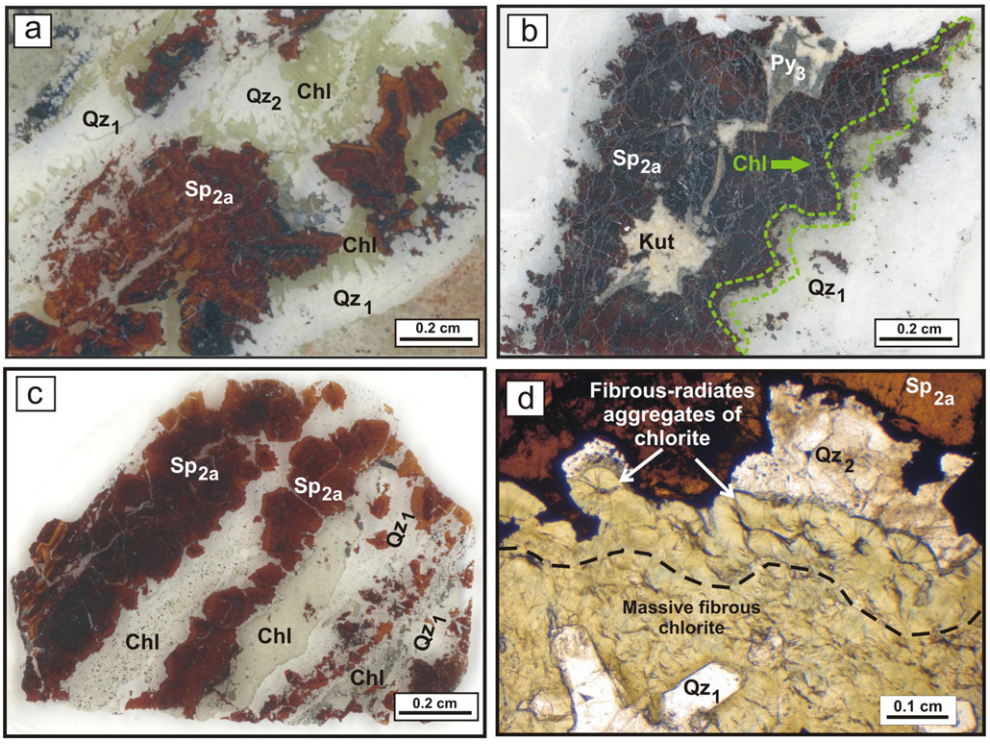

Fig. 2. Detailed photographs of thin sections: (a-b) chlorite postdating Qz_1 and coeval to Qz_2 and Sp2a within mineralised veins, and (c) chlorite interbedded with Sp2a. (d) Photomicrograph in transmitted light, one-polar, showing the two textural types of chlorite (massive fibrous chlorite and radiated aggregate of chlorite) within the mineralised vein. Qz_1 = Quartz stage 1; Qz_2 = Quartz stage 2; Sp2a = Sphalerite stage 2a; Py_3 = Pyrite stage 3; Chl = chlorite; Kut = Kutnohorite.

air dried, treated with ethylene glycol and heated to 550 °C/2 h and then analysed. Randomly oriented powders were scanned from 2 to 65° and oriented aggregates from 2 to 30° 2θ with a step size of 0.02°–2θ/s and counting time of 1 s per step.

From the 22 vein samples, polished thin sections of 15 samples containing more than 5 % of chlorite were prepared and studied under a petrographic microscope and a JEOL JSM-820 scanning electron microscope (SEM). The chemical composition of chlorite present in these samples was determined from electron probe microanalysis (EPMA) using a JEOL Superprobe JXA-8900 at the National Centre of Electronic Microscopy of the Complutense University of Madrid. Kα X-ray lines were measured for: Si, Al, Fe, Mn, Mg, Ca, Na, K, Ti, Ni, Cr, P, F and Cl. The accelerating voltage was 20 kV; 50 nA beam current and 1–5 μm beam diameter. Counting times ranged from 20 to 60 s. The following standards were used: albite (Si, Al), ilmenite (Fe, Ti), Mn and Ni metal (Mn, Ni), kaersutite (Mg), fluorapatite (Ca, F, P, Cl), scapolite (Na), microcline (K) and chromite (Cr) from the Smithsonian Institution and Harvard University (Jarosewich et al., 1980; McGuire et al., 1992). Qualitative compositional maps were also obtained with the JEOL Superprobe for Si, Al, Fe, Mn and Mg elements.

Four geothermometers based on thermodynamic criteria have been used here to estimate the temperature of formation of vein chlorite from electron microprobe analyses: the Bourdelle et al. (2013), Lanari et al. (2014) Chl (2), Vidal et al. (2005, 2006) and Inoue et al. (2009, 2010) geothermometers. Bourdelle geothermometer was tested on chlorite formed at temperatures lower than 350 °C and pressure lower than 4 kbar; and the Lanari Chl (2) geothermometer on chlorite formed at temperatures from 100 to 500 °C and pressure from 1 to 20 kbar. The semi-empirical Bourdelle et al. (2013) and Lanari et al. (2014) Chl (2) geothermometers are calibrated from natural cases, therefore they implicitly assume an average Fe^{3+}/Fe ratio; hence used formulae are calculated with all iron as ferrous. The Vidal et al. (2005, 2006) geothermometers calculates the most probable Fe^{3+}/Fe ratio for each analysis taking into account the intersection in the P/T space of various reactions among the different components of the chlorite plus quartz and water at a given pressure. A pressure of 1 kbar was assumed for the calculation. Inoue et al. (2009, 2010) geothermometer needs an external data about Fe^{3+}/Fe ratio: the same estimations of the Fe^{3+}/Fe ratio from the application of Vidal et al. (2005, 2006) geothermometer were used. All the geothermometric calculations were applied to chlorite free of smectitic interstratified layers ($Na + K + Ca < 0.1$ a.f.m.). According to Bourdelle and Cathelineau (2015) and Vidal et al. (2016) analyses having very low amount of octahedral vacancies produce erratic temperature estimations, affected by a significant margin of error; therefore only analyses with the sum of octahedral sites lower than 5.9 a.f.m were used for the final temperature estimation. In all the cases, chlorites need to be in equilibrium with quartz and water.

Data management and analysis were performed using the statistical software R 3.1.2 (R Core Team 2014). Qualitative data from Si, Al, Fe, Mn and Mg compositional maps of chlorite obtained in the JEOL Superprobe were transformed into quantitative contents using several EPMA data as calibration. These quantitative contents were used to estimate the temperature of formation of chlorite using the Bourdelle et al. (2013) and the Lanari et al. (2014) Chl (2) methods. Finally, compositional and geothermal maps of chlorite were plotted using the R function spplot of the sp package (Pebesma and Bivand, 2005; Bivand et al., 2013).

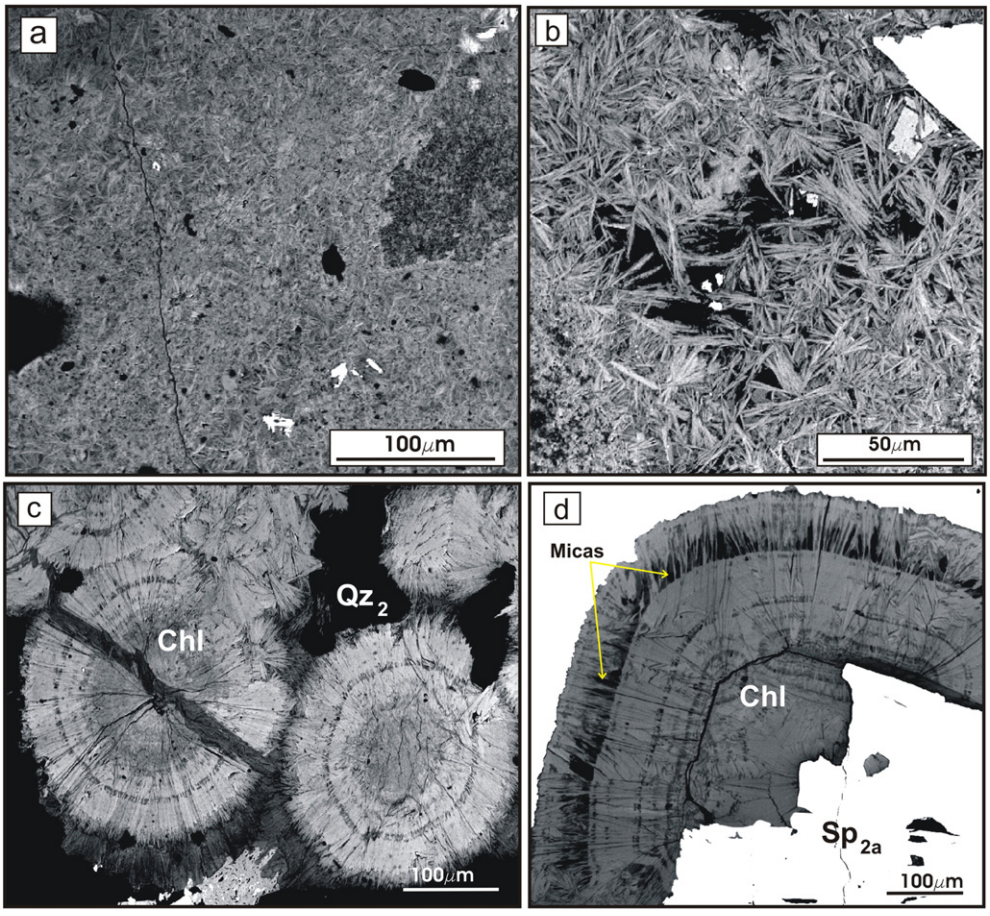

Fig. 3. EPMA photomicrographs showing the common aspect of the: (a) massive fibrous chlorite with darker and lighter areas, (b) detail of texture of massive fibrous chlorite, (c-d) fibrous –radiated aggregates of chlorite. Note in (d) an exterior band of mica interbedded within chlorite. Qz2 = Quartz stage 2; Sp2a = Sphalerite stage 2a; Chl = chlorite.

4. Results

4.1. Petrography

Vein chlorite is observed associated to the mineralised veins of the Patricia deposit. Chlorite in host rocks is also abundant as part of the hydrothermal alteration in the country rock. The detailed study of the vein chlorite is the object of this work. The most common occurrence of vein chlorite is forming massive aggregates (massive chlorite) of fibrous chlorite (Figs. 2a-b-c), although fibrous chlorite forming radiated aggregates (radiated chlorite) is also observed (Fig. 2d).

Massive chlorite, from veins boundaries inwards, is systematically observed postdating prismatic crystals of quartz formed at the end of the pre-ore stage (Figs. 2a-b). Towards the vein centre, massive chlorite outlines sphalerite bands and intergrowth in sphalerite and quartz of the substage 2a of the base-metal and silver stage (Fig. 2a). Furthermore, rhythmic banding formed by sphalerite of the substage 2a and massive chlorite are observed (Fig. 2c). Radiated chlorite is less abundant than massive chlorite and post-dates it (Fig. 2d).

SEM images shows dark and light areas in massive chlorite indicating compositional variations in the same fibre (Figs. 3a-b). Radiated chlorite also shows oscillatory zoning patterns under SEM (Figs 3c-d) with the presence of micas in the most external bands (Fig. 3d)

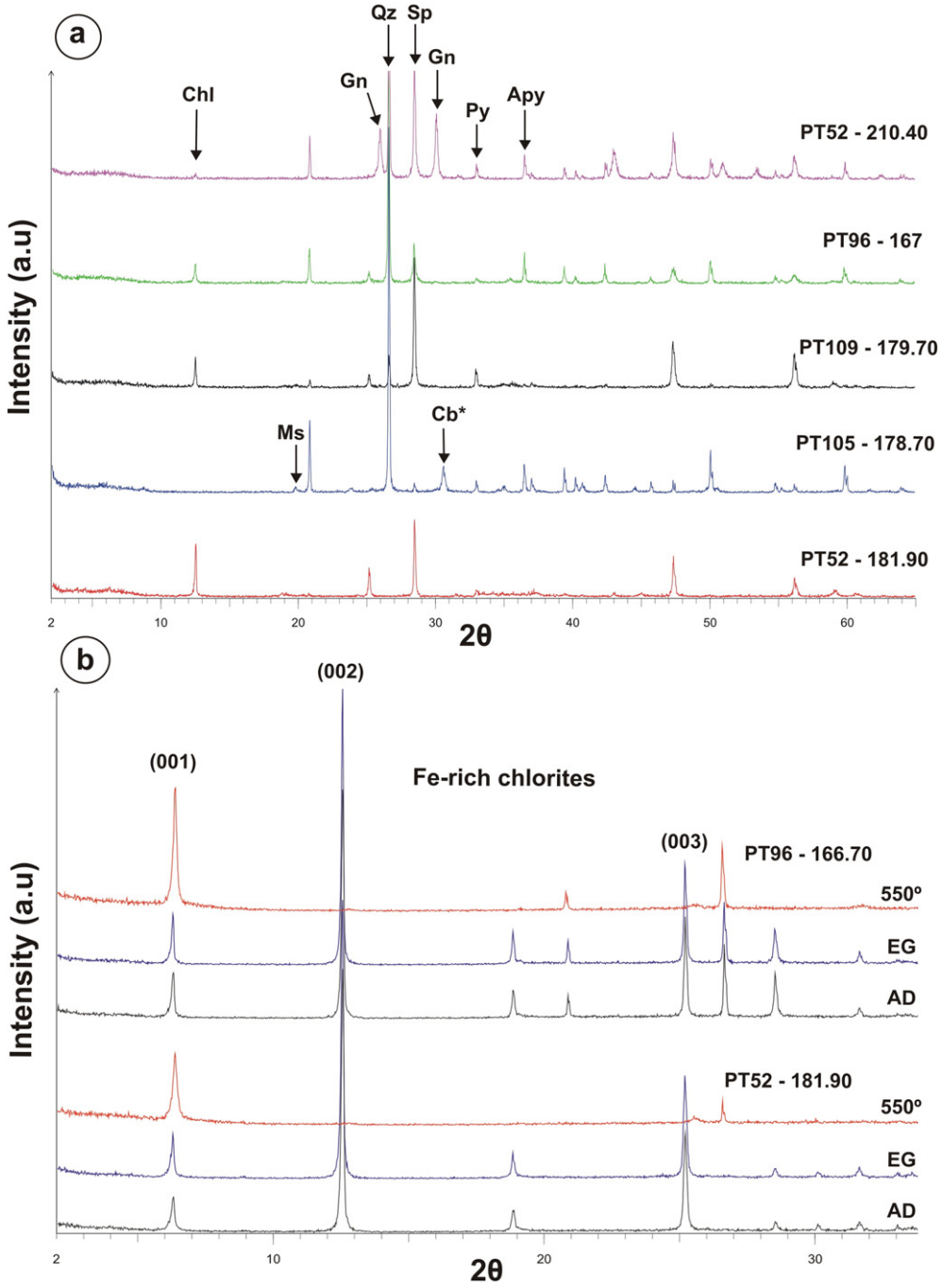

Fig. 4. a) Five representative powder mounts diffractograms showing the main mineralogy observed in the samples b) Two representative oriented aggregate mounts diffractograms of samples with chlorites. The Fe-rich chlorite was determined by the (002) reflection, which is more intense than the (001) reflection. Mineral abbreviations are according to Whitney and Evans (2010). Cb* = kutnohorite.

Table 1
Representative electron microprobe analyses of the massive fibrous chlorite crystals and the fibrous-radiated aggregates of chlorite.

	Massive fibrous chlorite												Fibrous-radiated aggregates of chlorite											
	PT52-182.16			PT96-166.70			PT96-167			PT105-178.70			PT96-167-Chl1				PT96-167-Chl2				PT96-167-Chl3			
													Light band		Dark band		Light band		Dark band		Light band		Dark band	
	3	8	14	16	26	31	55	78	82	93	100	101	2	4	7	11	39	47	43	55	66	77	64	88
Element																								
SiO2	23.82	24.24	26.69	24.81	23.41	22.52	23.85	24.15	23.49	23.02	23.56	23.18	23.84	24.11	23.78	24.25	23.00	23.47	23.15	23.05	22.94	23.29	23.28	23.97
Al2O3	19.84	21.99	21.82	21.65	20.45	20.53	20.10	21.24	21.29	20.63	20.27	20.82	21.44	20.82	21.92	21.06	21.15	20.66	21.55	21.07	20.83	21.01	21.45	21.32
FeO	33.94	28.46	28.61	28.08	33.56	35.30	39.63	38.47	34.65	39.79	37.50	38.44	39.61	40.56	32.37	37.02	36.43	38.62	33.69	32.77	38.41	39.62	33.76	34.78
MnO	5.38	7.49	1.87	5.43	4.68	4.17	2.26	3.16	6.44	2.07	2.64	3.12	2.21	2.29	6.33	3.64	4.87	2.92	5.58	6.88	2.66	2.56	5.55	5.57
MgO	3.76	5.61	7.68	4.76	4.50	3.48	1.46	2.18	3.45	1.31	2.08	1.88	1.70	1.43	4.13	2.38	3.17	1.99	4.14	4.42	1.96	1.62	3.70	3.12
CaO	0.06	0.03	0.03	0.13	0.01	0.03	0.03	0.03	0.01	0.05	0.08	0.04	0.02	0.02	0.03	0.02	0.03	–	0.03	0.04	0.03	–	0.05	0.07
Na2O	0.02	0.02	0.01	0.01	–	0.03	0.02	–	0.01	0.06	0.04	0.07	0.02	–	0.02	0.05	–	0.02	0.02	0.01	0.05	0.05	–	0.02
K2O	0.02	0.00	0.30	0.57	0.03	0.02	–	–	0.01	0.08	0.17	0.02	–	–	–	0.00	–	–	–	0.00	–	0.00	0.01	0.00
TiO2	0.55	0.05	0.06	0.07	0.05	0.03	0.04	0.04	0.04	0.04	0.05	0.02	0.01	–	0.01	–	0.01	0.03	0.05	0.03	–	–	0.00	–
NiO	0.00	–	–	–	–	0.07	0.03	0.04	0.03	–	–	–	0.01	0.06	0.01	0.01	0.03	–	–	0.08	0.02	–	0.05	–
Cr2O3	0.00	0.02	0.04	–	0.04	–	–	–	0.02	0.02	–	0.01	0.02	–	–	–	–	–	–	0.02	0.01	–	0.01	–
P2O5	0.00	–	–	–	–	0.01	0.05	–	–	0.01	0.01	0.02	0.01	–	0.01	–	0.01	–	–	0.03	0.02	0.03	0.02	–
F	0.01	–	0.02	–	0.02	–	–	–	–	–	–	0.00	–	–	–	0.05	–	–	–	–	–	–	–	–
Cl	0.03	0.02	0.02	0.01	0.02	0.00	0.03	0.03	0.02	0.04	0.03	0.03	0.03	0.01	0.06	0.06	0.02	0.02	0.04	0.04	0.02	0.02	0.05	0.03
Total	87.42	87.93	87.11	85.52	86.75	86.17	87.47	89.34	89.46	87.10	86.42	87.63	88.89	89.30	88.65	88.51	88.71	87.71	88.23	88.42	86.95	88.20	87.91	88.88
Apfu																								
Si	2.73	2.69	2.89	2.81	2.69	2.63	2.77	2.72	2.64	2.69	2.75	2.68	2.71	2.74	2.66	2.75	2.62	2.71	2.62	2.62	2.67	2.68	2.65	2.70
Al	2.68	2.88	2.79	2.89	2.77	2.83	2.75	2.82	2.83	2.84	2.79	2.84	2.87	2.79	2.89	2.82	2.84	2.81	2.88	2.82	2.86	2.85	2.88	2.83
Fe	3.25	2.64	2.59	2.66	3.22	3.45	3.84	3.63	3.26	3.89	3.66	3.72	3.76	3.86	3.03	3.51	3.47	3.73	3.19	3.11	3.74	3.82	3.21	3.28
Mn	0.52	0.71	0.17	0.52	0.46	0.41	0.22	0.30	0.61	0.21	0.26	0.31	0.21	0.22	0.60	0.35	0.47	0.29	0.54	0.66	0.26	0.25	0.53	0.53
Mg	0.64	0.93	1.24	0.80	0.77	0.61	0.25	0.37	0.58	0.23	0.36	0.32	0.29	0.24	0.69	0.40	0.54	0.34	0.70	0.75	0.34	0.28	0.63	0.52
Ca	0.00	0.00	0.00	0.00	0.00	0.00	0.00	0.00	0.00	0.00	0.00	0.00	0.00	0.00	0.00	0.00	0.00	0.00	0.00	0.00	0.00	0.00	0.00	0.00
Na	0.00	0.00	0.00	0.00	0.00	0.01	0.00	0.00	0.00	0.01	0.01	0.02	0.00	0.00	0.00	0.01	0.00	0.00	0.00	0.00	0.01	0.01	0.00	0.00
K	0.00	0.00	0.00	0.00	0.00	0.00	0.00	0.00	0.00	0.00	0.00	0.00	0.00	0.00	0.00	0.00	0.00	0.00	0.00	0.00	0.00	0.00	0.00	0.00
Ti	0.05	0.00	0.00	0.01	0.00	0.00	0.00	0.00	0.00	0.00	0.00	0.00	0.00	0.00	0.00	0.00	0.00	0.00	0.00	0.00	0.00	0.00	0.00	0.00
Ni	0.00	0.00	0.00	0.00	0.00	0.01	0.00	0.00	0.00	0.00	0.00	0.00	0.00	0.01	0.00	0.00	0.00	0.00	0.00	0.01	0.00	0.00	0.00	0.00
Cr	0.00	0.00	0.00	0.00	0.00	0.00	0.00	0.00	0.00	0.00	0.00	0.00	0.00	0.00	0.00	0.00	0.00	0.00	0.00	0.00	0.00	0.00	0.00	0.00
P	0.00	0.00	0.00	0.00	0.00	0.00	0.00	0.00	0.00	0.00	0.00	0.00	0.00	0.00	0.00	0.00	0.00	0.00	0.00	0.00	0.00	0.00	0.00	0.00
F	0.00	0.00	0.01	0.00	0.01	0.00	0.00	0.00	0.00	0.00	0.00	0.00	0.00	0.00	0.00	0.02	0.00	0.00	0.00	0.00	0.00	0.00	0.00	0.00
Cl	0.01	0.00	0.00	0.00	0.00	0.00	0.00	0.01	0.00	0.01	0.01	0.01	0.01	0.00	0.01	0.01	0.00	0.00	0.01	0.01	0.00	0.00	0.01	0.01
AlVI	1.41	1.57	1.68	1.70	1.46	1.46	1.52	1.55	1.47	1.53	1.54	1.52	1.58	1.53	1.56	1.57	1.46	1.52	1.50	1.43	1.53	1.53	1.52	1.53
AlIV	1.27	1.31	1.11	1.19	1.31	1.37	1.23	1.28	1.36	1.31	1.25	1.32	1.29	1.26	1.34	1.25	1.38	1.29	1.38	1.38	1.33	1.32	1.35	1.30
ΣVI	5.89	5.86	5.70	5.69	5.93	5.95	5.85	5.86	5.94	5.88	5.84	5.90	5.86	5.86	5.90	5.87	5.96	5.89	5.94	5.97	5.90	5.90	5.91	5.88
Σinter.	0.01	0.00	0.00	0.00	0.00	0.01	0.00	0.00	0.00	0.01	0.01	0.02	0.00	0.00	0.00	0.01	0.00	0.00	0.00	0.00	0.01	0.01	0.00	0.00

4.2. X-ray diffraction

XRD patterns of randomly oriented powder mounts show that the mineralogical association is composed of quartz, sphalerite, galena, pyrite, arsenopyrite, kutnohorite, micas and IIb-polytype chlorite in different amounts in each sample from the mineralised veins (Fig. 4a). The clay mineralogy was studied by XRD from oriented aggregate mounts of samples containing abundant chlorite. The data shows that they are Fe-rich chlorites (chamosite) based on the intensity of the (002) reflection in comparison with the (001) reflection (Fig. 4b). According to Inouá and Kogure (2016) the presence of Mn in the structure of the chlorites would affect their (002)/(001) intensity ratio in a similar manner to Fe. Additionally, comparison between air-dried and ethylene glycol treated specimens confirms the absence of expandable layers, both as discrete phases and as I/Sm or C/Sm mixed-layers (Fig. 4b).

4.3. Electron microprobe analyses

Electron microprobe analyses of chlorite were recalculated on the basis of 14 oxygens. Representative electron microprobe analyses of massive chlorite are listed in Table 1. The most important feature of these analyses is the high FeO content (average of 33 wt.%, standard deviation of 3.77 wt.% and up to 40 wt.%) confirming the results obtained in the semi-quantitative XRD results and classifying the vein chlorite of the Patricia deposit as chamosite. The average MnO content of massive chlorites is of 4.9 wt.% (standard deviation of 5.02 wt.%) and ranges from 1.87 to 7.49 wt.% The MgO content is similar to the MnO content with an average value of 4 wt.% (standard deviation of 1.47 wt.%) and ranges from 1.31 to 7.68 wt.%. MnO and MgO contents are higher and FeO content lower in the dark than the light areas of the fibres of massive chlorite. Moreover, MnO and MgO contents show a strong positive correlation ($r^2 = 0.78$, p-value = 0) and FeO content a strong negative correlation with MgO and MnO contents ($r^2 = 0.95$ and 0.82, p-value = 0, respectively). The SiO_2 and Al_2O_3 contents show a low variability (standard deviation of 0.54 and 0.64 wt.% respectively) with average contents of 23.65 and 20.98 wt.% respectively. CaO, K_2O, Na_2O, TiO_2, NiO and Cr_2O_3 average contents are lower than 0.05 wt.%.

Radiated chlorite shows similar composition to that of massive chlorite and can also be classified as chamosite. The oscillatory zoning of radiated chlorite was analysed from SiO_2, Al_2O_3, FeO, MnO and MgO compositional maps (Fig. 5). Compositional zoning consists on the formation of concentric bands with different contents on FeO, MgO and MnO whereas SiO_2 and Al_2O_3 contents remain invariable (Fig. 6). Light bands show higher FeO contents and lowers MnO and MgO contents than alternate dark bands. There are not significant variations from internal to external light or dark bands (Fig. 5). MnO and MgO contents in the light areas range from 1.72 to 2.54 wt.% and from 1 to 2.04 wt.% respectively, and FeO content ranges from 38.35 to 41.41 wt.%. In the dark areas, MnO content ranges from 3.29 to 9.32 wt.%, MgO from 2.34 to 5.44 wt.%, and FeO from 26.45 to 38.09 wt.%.

4.4. Chlorite as geothermometer

The Bourdelle et al. (2013), Lanari et al. (2014) Chl (2), Vidal et al. (2005, 2006) and Inoue et al. (2009, 2010) geothermometers were applied to each individual electron microprobe analysis of chlorite with (Na + K + Ca) < 0.1 in atoms per formula unit and octahedral sites below 5.90 (Table 2).

Temperatures estimated from massive chlorite are summarized in Table 2. The estimated mean temperature range from 188 °C for the Inoue geothermometer to 260 °C for the Lanari Chl (2) geothermometer. No significant differences in the temperatures estimated from light or dark areas of massive chlorite were observed.

Temperatures estimated from radiated chlorite are summarized in Table 2. The estimated mean temperature range from 213 °C for the Inoue geothermometer to 263 °C for the Lanari Chl (2) geothermometer. Mean temperatures estimated from radiated chlorite are similar than those estimated from massive chlorite (Table 2). Moreover, no significant variations on estimated temperatures are observed from core to rim of radiated chlorites nor between dark and light bands (Fig. 5). As Mn is not considered in the applied thermodynamic models, we have tried to repeat the calculations adding the Mn content alternatively to Fe or Mg. No significant differences have been found in the final results.

5. Discussion and conclusions

Chlorite is very abundant within the mineralised veins of the Patricia ore deposit. Before using chlorite as geothermometer, its position within the paragenetic sequence has to be fully clarified. In the paragenetic sequence estimated in previous works (Chinchilla et al., 2016), chlorite formed from the end of the pre-ore stage to the beginning of the post-ore stage with a maximum during the substage 2a. The detailed study of vein chlorite of the present work allows better constraining its position in the paragenetic sequence.

The spatial relationships among vein chlorite, quartz and sphalerite suggest that chlorite occurs at the end of the first stage and during the second stage. As described in the petrography section, massive chlorite is systematically observed postdating quartz of the pre-ore stage (Fig. 2a-b), and therefore its formation during the pre-ore stage is at least questionable. Massive chlorite outlines sphalerite bands, forms rhythmic banding with sphalerite and is intergrown with sphalerite and quartz of the substage 2a of the base-metal and silver stage, confirming the importance of the substage 2a in the formation of massive chlorite. Moreover, radiated chlorite post-dates massive chlorite and therefore radiated chlorite is suggested to have formed during the substage 2a but subsequently to the formation of massive chlorite. During the formation of sphalerite and galena of the substage 2b, chlorite is not observed and therefore the formation of chlorite is limited to the substage 2a. The conclusion is that massive chlorite formed at the beginning of the base-metal and silver stage and radiated chlorite at the end of the substage 2a, and the formation of chlorite during the pre-ore stage and the 2b substage should be discarded (Fig. 6)

Chlorite formed in the mineralised veins of the Patricia ore deposit can be classified as chamosite based on its content on FeO and XRD results from oriented aggregate mounts (Bayliss, 1975). Representative analyses of vein chlorite showed that Si contents range from 2.62 to 2.89 apfu and the sum of octahedral cations ($Al^{VI} + Fe^{2+} + Mg + Mn + Ti$) range from 5.69 and 5.96 apfu (Table 1). These compositional features are typical of low temperature chlorites (<300 °C) (Vidal et al., 2005; Inoue et al., 2009, 2010).

The special feature of the chlorite of the mineralised veins of the Patricia epithermal ore deposit is the high MnO contents (higher than 1.50 wt.% and up to 7.49 wt.%). Vein chlorite in epithermal ore deposits usually have MnO contents lower than 1 wt.%. (i.e. Salton Sea, McDowell and Elders, 1980; Los Azufres, Cathelineau, 1988; Bouillante, Mas et al., 2006; Tinguiririca, Vazquez et al., 2014), although MnO contents up to 3 wt.% have been reported (i. e. Creed district, Walshe, 1986; Broadlands - Ohaaki, De Caritat et al., 1993; Baguio, Cooke et al., 1996; Toyoha, Inoue et al., 2010).

These high MnO contents on vein chlorite may question the use of the geothermometers in the Patricia ore deposit. The chlorite

Fig. 5. Backscattered electron image taken at EPMA, compositional maps (SiO_2, Al_2O_3, FeO, MnO and MgO) and temperature maps (according to Lanari et al., 2014 and Bourdelle et al., 2013 methods) based on EPMA analyses on a representative radiated-chlorite.

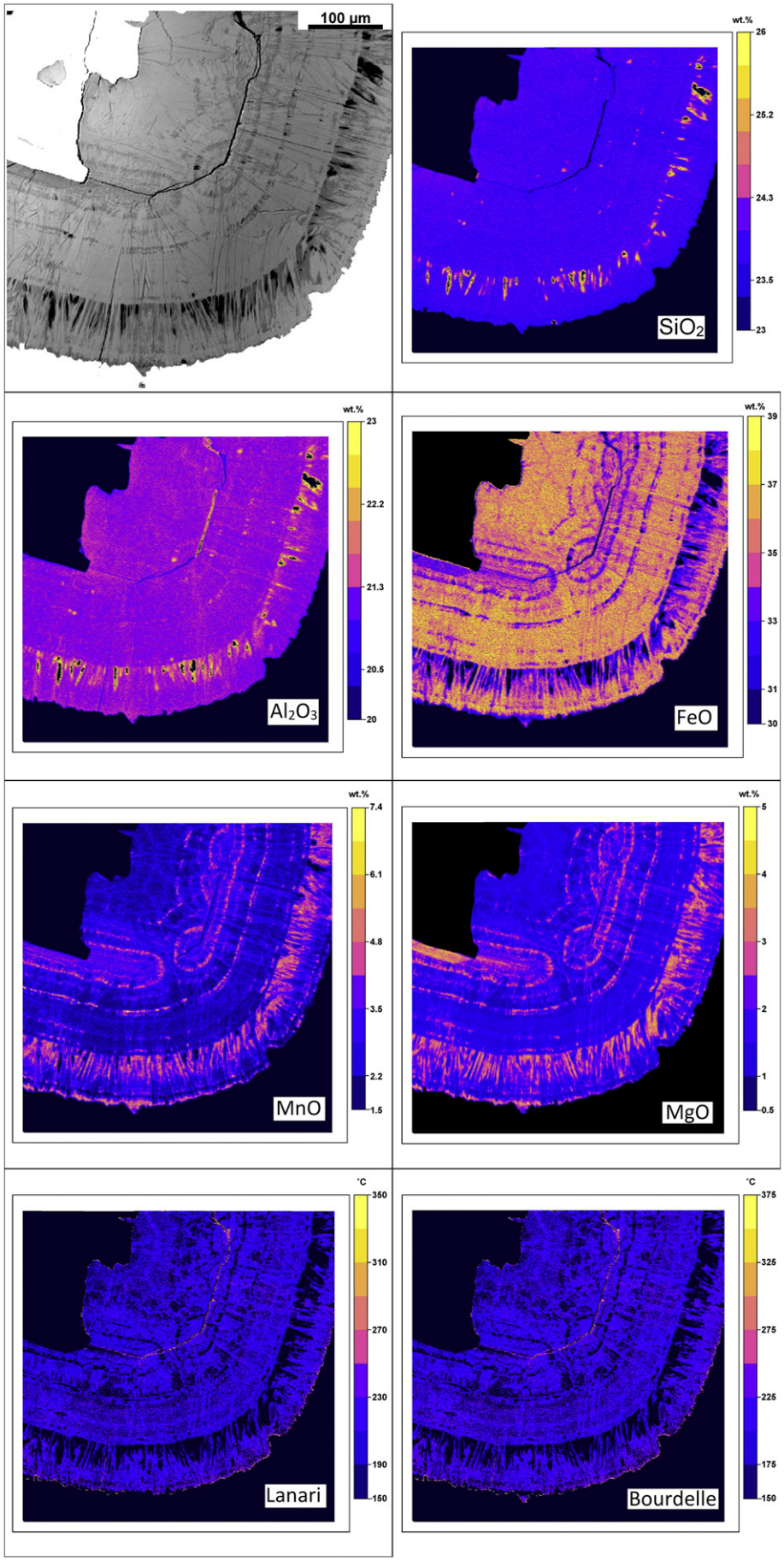
100 µm
wt.%
26
25.2
24.3
23.5
23
SiO2
wt.%
23
22.2
21.3
20.5
20
Al2O3
wt.%
39
37
35
33
31
30
FeO
wt.%
7.4
6.1
4.8
3.5
2.2
1.5
MnO
wt.%
5
4
3
2
1
0.5
MgO
°C
350
310
270
230
190
150
Lanari
°C
375
325
275
225
175
150
Bourdelle

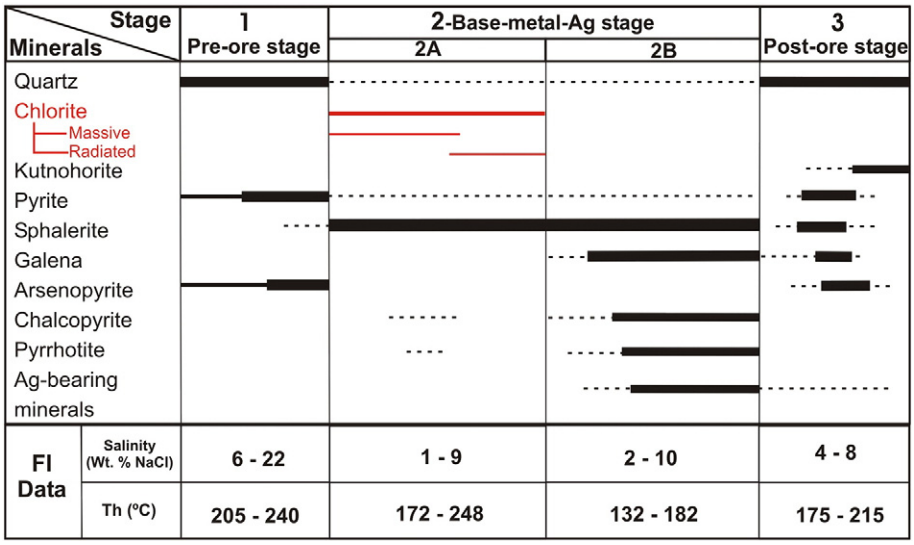

Fig. 6. Mineral assemblages and paragenetic sequence of the mineralised veins in the Patricia Zn-Pb-Ag epithermal deposit (modified from Chinchilla et al., 2016). Salinities and homogenisation temperatures estimated for each stage (Th) from fluid inclusion data are presented in the box below. Thick bars indicate higher abundances, thin and dashed lines refer to lower abundances.

Table 2
Summary of the estimated temperatures (mean, 95% interval for the mean, standard deviation, minimum and maximum) for massive and radiated chlorites based on Bourdelle et al. (2013), Lanari et al. (2014), Vidal et al. (2006) and Inoue et al. (2009, 2010) methods.

	n	Mean	95% interval		Standard deviation	Minimum	Maximum
			Lower	Upper			
Bourdelle et al. (2013)							
Massive chlorite	31	247	241	254	35	156	299
Radiated chlorite	62	250	247	254	25	192	298
Lanari et al. (2014) Chl(2)							
Massive chlorite	31	260	254	266	33	152	305
Radiated chlorite	62	263	259	267	30	179	308
Vidal et al. (2006)							
Massive chlorite	31	256	250	261	30	167	307
Radiated chlorite	62	257	254	261	26	180	299
Inoue et al. (2010)							
Massive chlorite	31	188	183	192	25	142	241
Radiated chlorite	62	213	210	216	22	167	259

geothermometers were successfully applied to vein chlorite with MnO contents lower than 1 wt.%. (e.g. Vazquez et al., 2014, Trincal et al., 2015; Zajzon et al., 2015; Hässig et al., 2015). They were based on thermodynamic models in the system SiO_2-Al_2O_3-FeO-MgO-H_2O and therefore do not consider the role of MnO in the estimation of the temperature. Schreyer et al. (1986) and Abad-Ortega and Nieto (1995) proved the existence of a compositional gap between Mg and Mn in chlorites of Sierra Albarrana, which indicates some structural differences between chlorites with low and high MnO contents and therefore different thermodynamic properties would be expected. To our knowledge, thermodynamic properties of a theoretical Mn-chlorite end-member have not yet been published. Therefore, all the published chlorite geothermometers consider only the end-members based on the simplest composition, having SiO_2, Al_2O_3, FeO, MgO and H_2O. Very recently, a new end-member containing Fe_2O_3 has been proposed (Trincal and Lanari, 2016) and considered in the thermodynamic formulation (Vidal et al., 2016).

For the geothermometers that do not need the Fe^{3+}/Fe ratio, the temperatures estimated from massive and radiated chlorites range from 156 to 299 °C and from 192 to 298 °C, respectively, for the Bourdelle geothermometer whereas for the Lanari Chl (2) geothermometer range from 152 to 305 °C and from 179 to 308, respectively. There are no significant differences between dark and light areas. Besides, these results have been compared with the geothermometers of Vidal et al. (2006) and Inoue et al. (2009), Inoue et al., 2010) where the knowledge of the Fe^{3+}/Fe ratio in chlorite is mandatory. The temperatures estimated with Vidal et al. (2006) range between 167 to 307 °C and 180 to 299 °C for massive and radiated chlorites, whereas with the method of Inoue et al. (2009) range between 142 to 241 °C and 167 to 259 °C, respectively (Table. 2). These temperature values from massive and radiated chlorite using the Vidal et al. (2006) geothermometer are similar to the values estimated with Bourdelle and Lanari Chl (2) methods, with an average of 256 and 258 °C for massive and radiated chlorite, respectively. This conclusion is in agreement with Vidal et al. (2016) for low pressure chlorites. For the Inoue geothermometer, the estimated temperatures are lower with average values of 188 and 213 °C for massive and radiated chlorite, respectively. Such difference could be influenced by the estimation of Fe^{3+}/Fe used for the Inoue et al. (2009) geothermometer from the data obtained by the Vidal et al. (2005, 2006) one. These two geothermometers use different crystal chemical assumptions and therefore the use of partial data of the latter for the former could be questionable.

The chlorite precipitation in the Patricia ore deposit, as indicated above, mainly took place during the substage 2a. In detail, the massive chlorite precipitated before the radiated chlorite and occurred close or interbedded in the sphalerite and quartz of the substage 2a (Fig. 2a-d). Temperatures estimated for the formation of sphalerite of the substage 2a from fluid inclusion data were from 172 to 248 °C (Chinchilla et al., 2015) (Fig. 6).

In order to compare estimated temperature from fluid inclusions and those obtained from the chlorite geothermometry, the temperatures estimated from the different geothermometers (Bourdelle, Lanari Chl (2), Vidal and Inoue) were represented against the octahedral vacancies (Fig.7). In this figure, it can be observed the relationship between temperature and octahedral vacancies, and how the temperature increase as the vacancy values decrease. According to Vidal et al. (2016) and Bourdelle and Cathelineau (2015), temperatures obtained from chlorites having less than 0.05 or 0.1 vacancies, respectively, are highly affected by small analytical and thermodynamic errors and they should be interpreted only as a maximum value. If we assume in Fig. 7 the lower limit of vacancy on 0.1, most of the temperature values are below 300 °C and the mean value is also below 260 °C. The approximated area of temperatures estimated from fluid inclusion has been

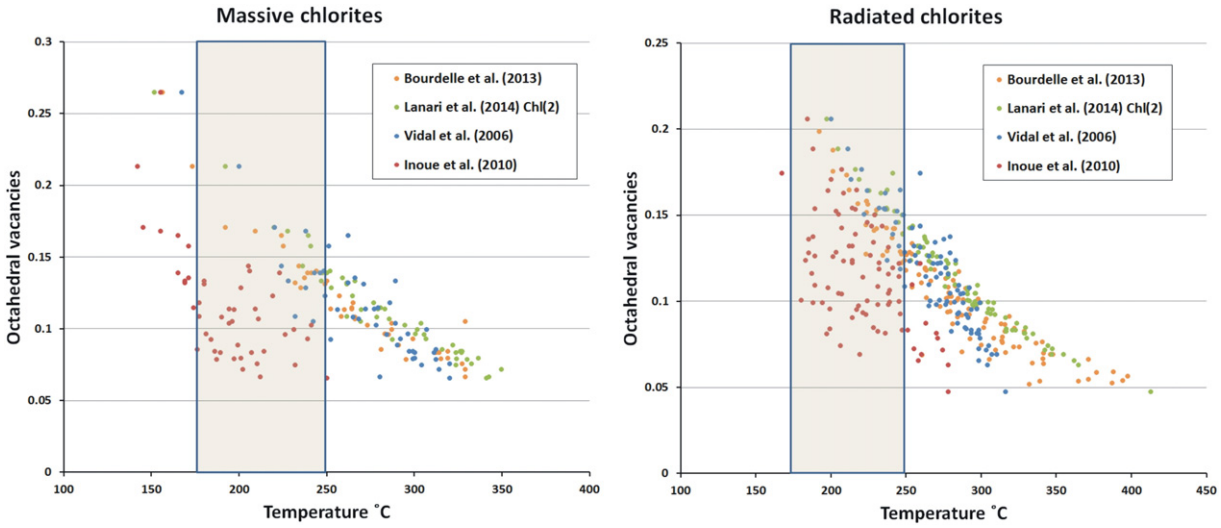

Fig. 7. Diagram representing the estimated temperatures for the used geothermometers against the octahedral vacancies for massive chlorites and radiated chlorites of the Patricia ore deposit. The shaded area represents the range of temperature previously estimated from fluid inclusion in sphalerite (Sp2a).

added to the graphic in Fig. 7 indicating a general coexistence of chlorite with the formation of sphalerite (Sp2a) during sub-stage 2a (Fig. 6). Nonetheless, both the crude analytical data and their interpretation by means of the four geothermometers indicate a significant scattering of values (Table 1, 2 and Fig. 7), also present in part in the fluid inclusion determinations. Therefore temperature is expected to have varied during the hydrothermal influx or for the different local places, having reached in some places or time higher values than those recorded by the fluid inclusions.

Therefore, the use of the massive and radiated chlorite as geothermometer in the mineralised veins of Patricia is in general coherent with the temperatures determined on fluid inclusions of sphalerite. Apparently, the high MnO contents of massive chlorite have not significantly affected their use as geothermometer, at less for this set of data, although any conclusion on this aspect should be contrasted by thermodynamic modelling of the Mn chlorite.

The formation of radiated chlorite (Fig. 5), also so-called oscillatory-zoned chlorite, is extremely rare in ore deposits and its use for geothermometric estimations has been already proved (i.e. Trincal et al., 2015). The formation of radiated chlorite subsequently to the massive chlorite indicates the existence of different pulses of mineralisation within the substage 2a. The concentric bands that form the oscillatory zoning of radiated chlorite indicate that these pulses had different Fe, Mn and Mg contents but similar temperatures.

In conclusion, this study confirms the applicability of the chlorite geothermometer in this type of paragenesis and its usefulness to characterise the thermal evolution in epithermal deposits as the Patricia ore deposit. The presence of important contents of Mn within chlorite has not affected their use as geothermometer. The similar estimated temperatures between the two types of vein chlorite and its different position in the paragenetic sequence indicate that its formation was controlled by fluid compositional variations but not by thermal conditions.

Acknowledgements

This work was made possible by Herencia Resources Plc., which provided access to drill core and geologic information. Appreciation is expressed to the technical staff of Herencia Resources Plc. at the Patricia deposit, for their assistance during our studies of the deposit. We would like to thank A. Larios from the Centro Nacional de Microscopía Electrónica in the Complutense University of Madrid for their assistance with the electron microprobe in the chemical analyses of the minerals. We thank to the Associate Editor Emilio Galan and the reviewers, Olivier Vidal and Atsuyuki Inoue whose comments and suggestions have largely contributed to improve the paper. Olivier Vidal is also thanked for his invaluable help with the geothermometric calculations. This research was financially supported by the project CGL2010 – 17668 of the Ministerio de Economía y Competitividad of Spain.

References

Abad-Ortega, M.M., Nieto, F., 1995. Extension and closure of the compositional gap between Mn-and Mg-rich chlorites toward Fe-rich compositions. Eur. J. Mineral. 363–368 http://dx.doi.org/10.1127/ejm/7/2/0363.
Bayliss, P., 1975. Nomenclature of the trioctahedral chlorites. Can. Mineral. 13, 178–180.
Behn, G., Camus, F., Carrasco, P., 2001. Aeromagnetic signature of porphyry copper systems in northern Chile and its geologic implications. Econ. Geol. 96, 239–248. http://dx.doi.org/10.2113/gsecongeo.96.2.239.
Bivand, R.S., Pebesma, E., Gómez-Rubio, V., 2013. Spatial Data Import and Export. Springer, New York, pp. 83–125.
Bourdelle, F., Cathelineau, M., 2015. Low-temperature chlorite geothermometry: a graphical representation based on a T–R2+–Si diagram. Eur. J. Mineral. 27, 617–626. http://dx.doi.org/10.1127/ejm/2015/0027-2467.
Bourdelle, F., Parra, T., Chopin, C., Beyssac, O., 2013. A new chlorite geothermometer for diagenetic to low-grade metamorphic conditions. Contrib. Mineral. Petrol. 165, 723–735. http://dx.doi.org/10.1007/s00410-012-0832-7.
Camus, F., Dilles, J.H., 2001. A special issue devoted to porphyry copper deposits of northern Chile. Econ. Geol. 96, 233–238. http://dx.doi.org/10.2113/gsecongeo.96.2.233.
Cathelineau, M., 1988. Cation site occupancy in chlorites and illites as function of temperature. Clay Miner. 23, 471–485.
Cathelineau, M., Nieva, D., 1985. A chlorite solid solution geothermometer the Los Azufres (Mexico) geothermal system. Contrib. Mineral. Petrol. 91, 235–244.
Chinchilla, D., Rodríguez, A., Piña, R., Ortega, L., Lunar, R., Quesada, C., Valverde, A., 2013. A mineralogical and fluid inclusion study of the Patricia Zn-Pb-Ag Deposit (Paguanta, NE Chile). Proceedings of the 12th Biennial SGA meeting. 2, pp. 786–788 Uppsala, Sweden.
Chinchilla, D., Ortega, L., Piña, R., Merinero, R., Bodnar, R.J., Moncada, D., Lunar, R., 2015. Fluid evolution in the Patricia Zn-Pb-Ag vein deposit (Paguanta, NE Chile): fluid inclusion assemblages and laser ablation ICP-MS evidence. Proceedings of the 13th SGA Biennial Meeting. 2, pp. 437–440 Nancy, France.
Chinchilla, D., Ortega, L., Piña, R., Merinero, R., Moncada, D., Bodnar, R.J., Quesada, C., Valverde, A., Lunar, R., 2016. The Patricia Zn-Pb-Ag epithermal ore deposit: an uncommon type of mineralization in northeastern Chile. Ore Geol. Rev. 73, 104–126.
Cooke, D.R., McPhail, D.C., Bloom, M.S., 1996. Epithermal gold mineralization, Acupan, Baguio District, Philippines; geology, mineralization, alteration, and the thermochemical environment of ore deposition. Econ. Geol. 91, 243–272. http://dx.doi.org/10.2113/gsecongeo.91.2.243.
De Caritat, P., Hutcheon, I., Walshe, J.L., 1993. Chlorite geothermometry: a review. Clay Clay Miner. 41, 219–239.
Dora, M.L., Randive, K.R., 2015. Chloritisation along the Thanewasna shear zone, Western Bastar Craton, Central India: Its genetic linkage to Cu–Au mineralisation. Ore Geol. Rev. 70, 151–172. http://dx.doi.org/10.1016/j.oregeorev.2015.03.018.
Essene, E.J., Peacor, D.R., 1995. Clay mineral thermometry - a critical perspective. Clay Clay Miner. 43, 540–553.

Hässig, M., Rolland, Y., Sosson, M., Avagyan, A., 2015. Lithological Nature of the Subduction Channel: Insights from the Karabakh Suture Zone (Lesser Caucasus) and General Comparisons J. Geodyn http://dx.doi.org/10.1016/j.jog.2015.07.006.
Hayes, J.B., 1970. Polytypism of chlorite in sedimentary rocks. Clay Clay Miner. 18, 285–306.
Hillier, S., Velde, B., 1991. Octahedral occupancy and the chemical composition of diagenetic (low-temperature) chlorite. Clay Miner. 26, 149–168.
Inouá, S., Kogure, T., 2016. High-Resolution Transmission Electron Microscopy (HRTEM) study of stacking irregularity in Fe-rich chlorite from selected hydrothermal ore deposits. Clay Clay Miner. 64, 131–144.
Inoue, A., Meunier, A., Patrier-Mas, P., Rigault, C., Beaufort, D., Vieillard, P., 2009. Application of chemical geothermometry to low-temperature trioctahedral chlorites. Clay Clay Miner. 57, 371–382. http://dx.doi.org/10.1346/CCMN.2009.0570309.
Inoue, A., Kurokawa, K., Hatta, T., 2010. Application of chlorite geothermometry to hydrothermal alteration in Toyoha geothermal system, southwestern Hokkaido, Japan. Resour. Geol. 60, 52–70. http://dx.doi.org/10.1111/j.1751-3928.2010.00114.x.
Jarosewich, E., Nelen, J.A., Norberg, J.A., 1980. Reference samples for electron microprobe analysis. Geostand. Newslett. 4, 43–47.
Kranidiotis, P., MacLean, W.H., 1987. Systematics of chlorite alteration at the Phelps Dodge massive sulfide deposit, Matagami, Quebec. Econ. Geol 82, 1898–1911.
Lanari, P., Wagner, T., Vidal, O., 2014. A thermodynamic model for di-trioctahedral chlorite from experimental and natural data in the system MgO–FeO–Al_2O_3–SiO_2–H_2O: applications to P–T sections and geothermometry. Contrib. Mineral. Petrol. 167, 1–19. http://dx.doi.org/10.1007/s00410-014-0968-8.
Lonsdale, P., 2005. Creation of the Cocos and Nazca plates by fission of the Farallon plate. Tectonophysics 404, 237–264. http://dx.doi.org/10.1016/j.tecto.2005.05.011.
López-Munguira, A., Nieto, F., Morata, D., 2002. Chlorite composition and geothermometry: a comparative HRTEM/AEM-EMPA-XRD study of Cambrian basic lavas from the Ossa Morena Zone, SW Spain. Clay Miner. 37, 267–281. http://dx.doi.org/10.1180/0009855023720033.
Maksaev, V., Townley, B., Palacios, C., Camus, F., 2007. Metallic ore deposits. In: Gibbons, W. (Ed.), Moreno T. The Geology of Chile, The Geological Society of London, pp. 179–199.
Martinod, J., Husson, L., Roperch, P., Guillaume, B., Espurt, N., 2010. Horizontal subduction zones, convergence velocity and the building of the Andes. Earth Planet. Sci. Lett. 299, 299–309. http://dx.doi.org/10.1016/j.epsl.2010.09.010.
Mas, A., Guisseau, D., Mas, P.P., Beaufort, D., Genter, A., Sanjuan, B., Girard, J.P., 2006. Clay minerals related to the hydrothermal activity of the Bouillante geothermal field (Guadeloupe). J. Volcanol. Geotherm. Res. 158, 380–400. http://dx.doi.org/10.1016/j.jvolgeores.2006.07.010.
McDowell, S.D., Elders, W.A., 1980. Authigenic layer silicate minerals in borehole Elmore 1, Salton Sea geothermal field, California, USA. Contrib. Mineral. Petr. 74, 293–310.
McGuire, A.V., Francis, C.A., Dyar, M.D., 1992. Mineral standards for electron microprobe analysis of oxygen. Am. Mineral. 77, 1087–1091.
Moore, D.M., Reynolds, R.C., 1989. X-ray diffraction and the identification and analysis of clay minerals. Oxford university press, Oxford, p. 378.
Parra, T., Vidal, O., Theye, T., 2005. Experimental data on the Tschermak substitution in Fe-chlorite. Am. Mineral. 90, 359–370. http://dx.doi.org/10.2138/am.2005.1556.
Pebesma, E.J., Bivand, R.S., 2005. Classes and methods for spatial data in R. R News 5 (2)http://cran.r-project.org/doc/Rnews/.
Rae, A.J., O'Brien, J., Ramirez, E., Bignall, G., 2011. The application of chlorite geothermometry to hydrothermally altered Rotokawa Andesite, Rotokawa Geothermal Field. NZ Geothermal Workshop, Proc. NZ Geotherm. Workshop. 33(6).
Schreyer, W., Fransolet, A.M., Abraham, K., 1986. A miscibility gap in trioctahedral Mn-Mg-Fe chlorites: evidence from the Lienne Valley manganese deposit, Ardennes, Belgium. Contrib. Mineral. Petr. 94, 333–342.
Sillitoe, R.H., Perelló, J., 2005. Andean copper province: tectonomagmatic settings, deposit types, metallogeny, exploration, and discovery. Econ. Geol. 845–890 100th Anniversary.
Silver, P.G., Russo, R.M., Lithgow-Bertelloni, C., 1998. Coupling of South American and African plate motion and plate deformation. Science 279, 60–63.
Trincal, V., Lanari, P., 2016. Al-free di-trioctahedral substitution and a ferri-sudoite end-member evidenced in chlorite. Clay Miner, Submitted.
Trincal, V., Lanari, P., Buatier, M., Lacroix, B., Charpentier, D., Labaume, P., Muñoz, M., 2015. Temperature micro-mapping in oscillatory-zoned chlorite: Application to study of a green-schist facies fault zone in the Pyrenean Axial Zone (Spain). Am. Mineral. 100, 2468–2483. http://dx.doi.org/10.2138/am-2015-5217.
Vazquez, M., Nieto, F., Morata, D., Droguett, B., Carrillo-Rosua, F.J., Morales, S., 2014. Evolution of clay mineral assemblages in the Tinguiririca geothermal field, Andean Cordillera of central Chile: an XRD and HRTEM-AEM study. J. Volcanol. Geotherm. Res. 282, 43–59. http://dx.doi.org/10.1016/j.jvolgeores.2014.05.022.
Vidal, O., Parra, T., Trotet, F., 2001. A thermodynamic model for Fe-Mg aluminous chlorite using data from phase equilibrium experiments and natural pelitic assemblages in the 100 to 600 °C, 1 to 25 kb range. Am. J. Sci. 301, 557–592.
Vidal, O., Parra, T., Vieillard, P., 2005. Thermodynamic properties of the Tschermak solid solution in Fe-chlorite: Application to natural examples and possible role of oxidation. Am. Mineral. 90, 347–358. http://dx.doi.org/10.2138/am.2005.1554.
Vidal, O., De Andrade, V., Lewin, E., Munoz, M., Parra, T., Pascarelli, S., 2006. P–T-deformation-Fe3 +/Fe2 + mapping at the thin section scale and comparison with XANES mapping: application to a garnet-bearing metapelite from the Sambagawa metamorphic belt (Japan). J. Metamorph. Geol. 24, 669–683. http://dx.doi.org/10.1111/j.1525-1314.2006.00661.x.
Vidal, O., Lanari, P., Muñoz, M., Bourdelle, F., de Andrade, V., 2016. Temperature, pressure, oxygen activity conditions of chlorite formation. Clay Miner.
Walker, J.R., 1993. Chlorite polytype geothermometry. Clay Clay Miner. 41, 260–267.
Walshe, J.L., 1986. A six-component chlorite solid solution model and the conditions of chlorite formation in hydrothermal and geothermal systems. Econ. Geol. 81, 681–703.
Whitney, D.L., Evans, B.W., 2010. Abbreviations for names of rock-forming minerals. Am. Mineral. 95, 185.
Xie, X., Byerly, G.R., Ferrell Jr., R.E., 1997. IIb trioctahedral chlorite from the Barberton greenstone belt: crystal structure and rock composition constraints with implications to geothermometry. Contrib. Mineral. Petrol. 126, 275–291.
Zajzon, N., Szentpéteri, K., Szakáll, S., Kristály, F., 2015. The origin of the Avram Iancu U–Ni–Co–Bi As mineralization, Băiţa (Bihor) metallogenic district, Bihor Mts., Romania. Int. J. Earth Sci. 104, 1865–1887. http://dx.doi.org/10.1007/s00531-015-1175-1.